

Going Off-Grid: Continuous Implicit Neural Representations for 3D Vascular Modeling

Dieuwertje Alblas¹(✉), Christoph Brune¹,
Kak Khee Yeung^{2,3}, and Jelmer M. Wolterink¹

¹ Department of Applied Mathematics, Technical Medical Centre,
University of Twente, Enschede, The Netherlands

d.alblas@utwente.nl

² Department of Surgery, Amsterdam UMC location Vrije Universiteit Amsterdam,
Amsterdam, The Netherlands

³ Amsterdam Cardiovascular Sciences, Microcirculation,
Amsterdam, The Netherlands

Abstract. Personalised 3D vascular models are valuable for diagnosis, prognosis and treatment planning in patients with cardiovascular disease. Traditionally, such models have been constructed with explicit representations such as meshes and voxel masks, or implicit representations such as radial basis functions or atomic (tubular) shapes. Here, we propose to represent surfaces by the zero level set of their signed distance function (SDF) in a differentiable implicit neural representation (INR). This allows us to model complex vascular structures with a representation that is implicit, continuous, light-weight, and easy to integrate with deep learning algorithms. We here demonstrate the potential of this approach with three practical examples. First, we obtain an accurate and watertight surface for an abdominal aortic aneurysm (AAA) from CT images and show robust fitting from as little as 200 points on the surface. Second, we simultaneously fit nested vessel walls in a single INR without intersections. Third, we show how 3D models of individual arteries can be smoothly blended into a single watertight surface. Our results show that INRs are a flexible representation with potential for minimally interactive annotation and manipulation of complex vascular structures.

Keywords: Implicit neural representation · Vascular model · Abdominal aortic aneurysm · Signed distance function · Level set

1 Introduction

Accurate and patient-specific models of vascular systems are valuable for diagnosis, prognosis and treatment planning in patients with cardiovascular disease. Personalised vascular models might be used for stent-graft sizing in patients with abdominal aortic aneurysms [27] or for computational fluid dynamics (CFD) [29]. However, extracting these models from medical image data can be cumbersome. Commercial software and open-source software packages [2, 3, 15] traditionally rely on the construction of tubular models [24] in three steps. First, the lumen

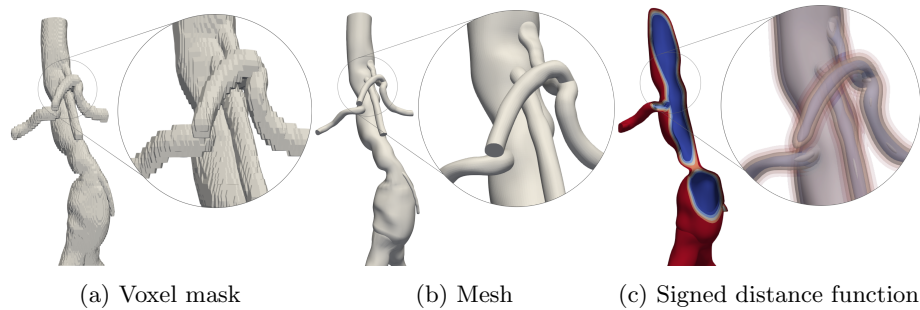


Fig. 1: Different representations of a 3D aortofemoral tree [30]. (a) and (b) are *explicit* representations; (a) has non-smooth boundaries, whereas boundaries of (b) are locally smooth. Both (a) and (b) are restricted to this resolution. (c) *implicitly* represents the surface with smooth boundaries, at any resolution.

centerline is identified for each vessel. Then, local cross-sectional contours are determined and used to construct a watertight mesh model using (spline) interpolation. Finally, polygon mesh models of multiple vessels are blended to obtain a connected vascular tree. In this approach, tortuosity of the centerline can cause self-intersections of the orthogonal contours, resulting in surface folding of the final mesh model [9]. Moreover, smoothly connecting triangular meshes around bifurcations is challenging.

Deep learning has made great progress towards automatic model building from images [6, 16]. However, popular convolutional neural network-based methods return 3D voxel masks. Because voxel masks merely discretize an underlying continuous shape, their quality heavily depends on the resolution of the image data, and they are not guaranteed to be contiguous. Hence, voxel masks typically require additional processing steps before use in, e.g., CFD. There is a need for a vascular model shape representation that is continuous, modular, and can be easily integrated with existing deep learning methods.

In this work, we adapt the work of Gropp et al. [10] to model vascular systems as combinations of level sets of signed distance functions represented in differentiable neural networks. Implicit representations and level sets have a substantial history in both segmentation [4, 17] and 3D modeling [11, 14] of vascular structures. Recently, there have been significant advances in signal representations using neural networks, i.e., implicit neural representations (INRs) [1, 18, 19, 22, 26]. Continuous implicit neural representations of the signed distance function can be easily transformed into an explicit representation, while the inverse is not true (Fig. 1).

We here demonstrate that INRs are a potentially valuable tool to bridge the gap between vascular modeling and deep learning. First, we show how INRs can be used to reconstruct an implicit surface from a sparse point cloud and form an alternative to conventional annotation procedures. We evaluate the efficiency and robustness of this approach. Secondly, we show that we can use a single

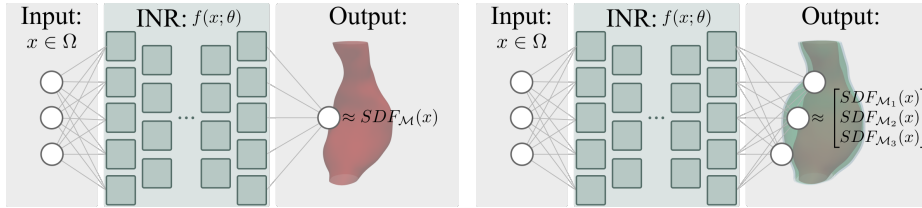


Fig. 2: Schematic overview of an implicit neural representation, parametrising a single SDF (left), or three SDFs simultaneously (right). Coordinate values can be queried and the network returns local SDF values.

INR to represent multiple surfaces, and demonstrate the effectiveness on nested shapes in an AAA case study. Finally, we demonstrate the added value of implicit shape representations in the smooth blending of separate structures in the reconstruction of an aortofemoral tree.

2 Method

We represent the surface of a vascular structure by the zero level set of its signed distance function (SDF), which we embed in a multilayer perceptron (MLP) as an implicit neural representation.

2.1 Signed distance functions

A surface can be *implicitly* described by the zero level set of its signed distance function (SDF). In the case of a 2D surface \mathcal{M} embedded in a 3D domain, $SDF_{\mathcal{M}}(\mathbf{x}) : \mathbb{R}^3 \rightarrow \mathbb{R}$ is defined as:

$$SDF_{\mathcal{M}}(\mathbf{x}) = \begin{cases} -d(\mathbf{x}, \mathcal{M}) & \mathbf{x} \text{ inside } \mathcal{M} \\ 0 & \mathbf{x} \text{ on } \mathcal{M} \\ d(\mathbf{x}, \mathcal{M}) & \mathbf{x} \text{ outside } \mathcal{M}, \end{cases} \quad (1)$$

$$\text{therefore: } \mathcal{M} = \{\mathbf{x} \in \mathbb{R}^3 | SDF_{\mathcal{M}}(\mathbf{x}) = 0\}. \quad (2)$$

In Eq. (1) $d(\mathbf{x}, \mathcal{M}) = \min_{\mathbf{y} \in \mathcal{M}} \|\mathbf{x} - \mathbf{y}\|$, the minimal distance to the surface. An SDF satisfies the Eikonal equation, hence $\|\nabla_x SDF_{\mathcal{M}}(\mathbf{x})\| = 1, \forall \mathbf{x}$. As this function is continuous on \mathbb{R}^3 , the surface \mathcal{M} is represented independently of resolution.

2.2 Implicit neural representations

Signed distance functions are often represented as a combination of SDFs of atomic shapes, or radial basis functions [5]. However, a recent insight shows that functions in space can be approximated using neural networks [22, 26]. These

so-called implicit neural representations (INRs) have been widely used for, e.g., image representations [7], novel view synthesis [19], image registration [32], and sparse-view CT reconstruction [28]. In this work, we use INRs to approximate the signed distance functions of one or multiple surfaces. This INR is a fully connected multilayer perceptron (MLP), $f(\mathbf{x}; \theta)$, that takes $\mathbf{x} \in \Omega := [-1, 1]^3 \subset \mathbb{R}^3$ as input, and outputs $SDF_{\mathcal{M}}(\mathbf{x})$, as shown in Figure 2(*left*). During optimization of the INR, desired properties of the SDF can be directly imposed on the network via the loss function. These properties include conditions on gradients and higher-order derivatives, as they can be computed for the network through backpropagation [26]. An INR thus represents a function or signal, and not a mapping between two functions, as is often the case with convolutional neural networks. As an INR is trained on continuous coordinates, they allow for representing a function at any resolution.

2.3 Optimizing an INR

We use an INR to represent the SDF of a 3D vascular model, under the condition that the model should be easily obtainable from a 3D medical image volume. We start from a small set of points on the vessel surface: $\mathcal{X} = \{\mathbf{x}_i\}_{i=1, \dots, N} \subset \Omega$. We aim to simultaneously reconstruct an SDF with \mathcal{X} on the zero levelset and embed it in an INR. This amounts to solving the Eikonal equation with pointwise boundary conditions; an ill-posed problem. Gropp et al. [10] tackle this ill-posedness by minimising the following loss function:

$$\ell(\theta) = \frac{1}{N} \sum_{1 \leq i \leq N} (|f(\mathbf{x}_i; \theta)|) + \lambda \mathbb{E}_{\mathbf{x}} (|\|\nabla_{\mathbf{x}} f(\mathbf{x}; \theta)\| - 1|^2). \quad (3)$$

The first term enforces that all points from \mathcal{X} lie on the zero level set of the SDF, and thus on the surface \mathcal{M} . The second term is a regularising term, encouraging that the INR $f(\mathbf{x}; \theta)$ satisfies the Eikonal equation, just like the SDF it represents. The key observation of Gropp et al. is that minimising Eq. (3) yields an SDF with a smooth and plausible zero isosurface. This approach allows for flexibility in the consistency of \mathcal{X} , in contrast to similar methods [20, 23], that require local normals or points to lie within the same plane. In Section 3.1, we investigate the quality and robustness of the reconstruction under variations of the point cloud.

2.4 Fitting multiple functions in an INR

The wall of blood vessels consists of layers, and in patients with abdominal aortic aneurysms (AAAs) the lumen and the surrounding solidified thrombus structure should be modeled separately [34]. While INRs have mostly been used to represent single functions, they can be extended to fit multiple functions on the same domain. Figure 2(*right*) visualizes how by adding additional output nodes to the neural network, multiple SDFs can be fitted simultaneously, in this

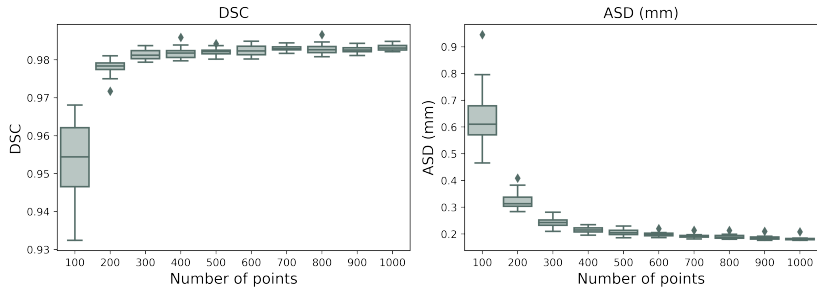


Fig. 3: The Dice similarity coefficient (DSC) and average surface distance (ASD) of reconstructed vascular surface for varying number of reference points. Each SDF is reconstructed using 20 different point clouds of each size.

case for the lumen, the inner wall, and outer wall of the AAA. This means that mutual properties of separate SDFs, such as for nested shapes, could be learned by a single neural network. This INR is optimised by minimising Eq. (3) on each of its output channels. We will compare this approach to multiple INRs representing structures separately in Section 3.2.

2.5 Constructive solid geometry

SDFs make it very easy to determine the union, difference, or intersection of multiple shapes, a cumbersome and challenging task in explicit polygon mesh representations [13,33]. Let $SDF_{\mathcal{M}_1}(\mathbf{x})$ and $SDF_{\mathcal{M}_2}(\mathbf{x})$ be SDFs for shapes \mathcal{M}_1 and \mathcal{M}_2 in Ω , respectively. Then their union is determined as:

$$\mathcal{M}_1 \cup \mathcal{M}_2 = \min(SDF_{\mathcal{M}_1}(\mathbf{x}), SDF_{\mathcal{M}_2}(\mathbf{x})) \quad (4)$$

To allow for smoother blending between interfaces of shapes, a smoothed min function can be considered [12]:

$$\begin{aligned} (\mathcal{M}_1 \cup \mathcal{M}_2)_{\text{smooth}} &= \min(SDF_{\mathcal{M}_1}(\mathbf{x}), SDF_{\mathcal{M}_2}(\mathbf{x})) - \gamma_{\text{smooth}}, \\ \gamma_{\text{smooth}} &= 0.25 \cdot k \cdot \max(k - |SDF_{\mathcal{M}_1}(\mathbf{x}) - SDF_{\mathcal{M}_2}(\mathbf{x})|, 0)^2, \end{aligned} \quad (5)$$

where k represents a smoothing parameter, i.e. a set region around the interfaces of the two surfaces. We will use this strategy to join structures represented by INRs in Section 3.3.

3 Experiments and Results

We conducted three experiments: (1) assessing the robustness of the INR against variations in the point cloud, (2) testing the effectiveness of representing multiple shapes with a single INR and (3) demonstrating how our method can be used to

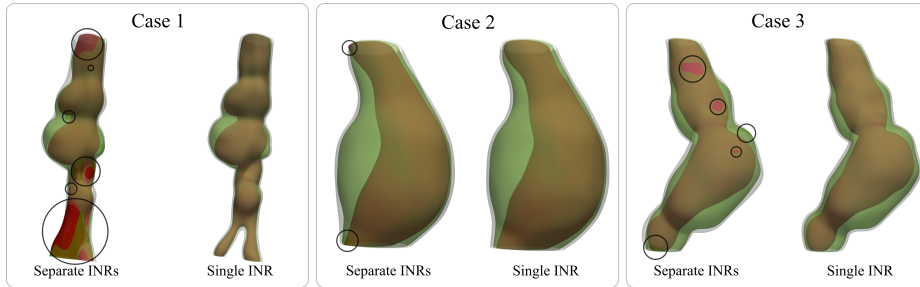


Fig. 4: Three nested AAA structures represented by a single INR, or separate INRs each representing a single shape. Using a single INR preserves the nested property, violations of this anatomical prior are marked with circles.

reconstruct a vascular system from separate vessels and blend them naturally. For all experiments we used MLPs consisting of an input layer with three nodes, six fully connected hidden layers with 256 nodes and ReLU activations, and a final prediction layer consisting of one or three nodes, embedding a single shape or three nested shapes respectively. Similar to [10], we used a skip connection, connecting the input to the third hidden layer. We base our implementation on PyTorch code⁴ provided with [10].

3.1 Robustness

We show how INRs can form an alternative to time-consuming annotation procedures, by fitting an SDF to a manually annotated point cloud. We assess the robustness against variations in this point cloud. We use a public dataset that contains 3D AAA meshes [31]. For each AAA, the dataset contains separate mesh representations for the lumen, the inner and outer vessel wall. For this experiment, we solely used the meshes of the lumen; we randomly sampled a set number of points on the mesh and repeated this sampling process 20 times, resulting in 20 different point clouds of the same size. For optimizing the INR, we used an Adam optimizer for 25,000 epochs, with a learning rate of 0.0001, and set λ in the loss function (Eq. (3)) to 0.1, as suggested in [10]. Optimisation was done on an NVIDIA Quadro RTX 6000 GPU, taking 10-15 minutes per network.

Figure 3 shows the quality of the surface lumen reconstruction in this model, in terms of the Dice similarity coefficient (DSC) and average surface distance (ASD). The DSC was computed using the original mesh as a reference, the ASD was computed using unseen points on the surface, i.e. points that were not in \mathcal{X} during optimisation. The median DSC is above 0.95 in all cases, even when only 100 points are used. We observe more variation in both metrics when the reconstruction is based on fewer points. Robustness and performance stabilize

⁴ <https://github.com/amosgropp/IGR>

after 400 points, implying that using more points will not further improve the quality or robustness of the reconstruction.

3.2 Reconstructing nested shapes

In our second experiment, we again use data provided in [31], with mesh representations for the lumen, inner wall, and outer wall of the aorta. Here, we aim to capture the nested property of the three shapes in the neural network representing their respective SDFs, meaning: $SDF_{\text{outer wall}}(\mathbf{x}) \leq SDF_{\text{inner wall}}(\mathbf{x}) \leq SDF_{\text{lumen}}(\mathbf{x})$, $\forall \mathbf{x} \in \Omega$. For each selected AAA case, we sampled a point cloud of 200 points for each of the three surfaces; a proper trade-off between point cloud sparsity and reconstruction quality. We fit a joint INR to these point clouds, as well as three separate INRs, one for each of the three surfaces. Figure 4 shows the resulting surfaces for both approaches. In all three cases, we see unwanted extrusions of the inner structures when separate INRs are used. Case 1 shows this effect best; the surfaces of the lumen and inner wall (red and green structures respectively) fail to capture the bifurcation and are inconsistent with the outer wall. In contrast, representation of the shapes using a single INR consistently resulted in none of these extrusions. Moreover, the thickness of the vessel wall remains constant for this approach, in agreement with ground-truth data.

3.3 Constructive geometry

In our third experiment, we demonstrate how INRs enable easy and smooth surface blending. This is critical for personalised vascular modeling, where many arteries of different calibers need to be blended into one single model for, e.g., CFD. Here, we use an aortofemoral tree from [30]. This sample consists of nine separate mesh structures: aorta, superior and inferior mesenteric arteries (SMA/IMA), renal arteries, hepatic artery, and common and internal iliac arteries, shown in Figure 5(*left*). For each of these mesh structures, we sample a point cloud of a size proportional to its surface area, to which we fit an INR, after normalizing it to the $[-0.9, 0.9]^3$ domain to allow for smooth blending. We optimize these networks using an Adam optimizer for 50,000 epochs.

To blend the vessels, we generate a Cartesian grid encompassing the entire vascular tree. Hence, this domain contains the respective subdomains that all nine INRs were trained on. To evaluate the INRs for each structure on this grid, we map each grid point to the corresponding coordinate in each INR domain and query the SDF value by forwarding it through the network. Next, we rescale the SDF value from the INR domain to the real size. This results in a grid containing patches of SDFs, that we blend together using Eq. (5), with smoothing parameter $k = 0.1$. The result in Figure 5(*right*) shows a smooth transition between the different vascular structures, without any intrusions on the inside, making this structure suitable for CFD analysis [14].

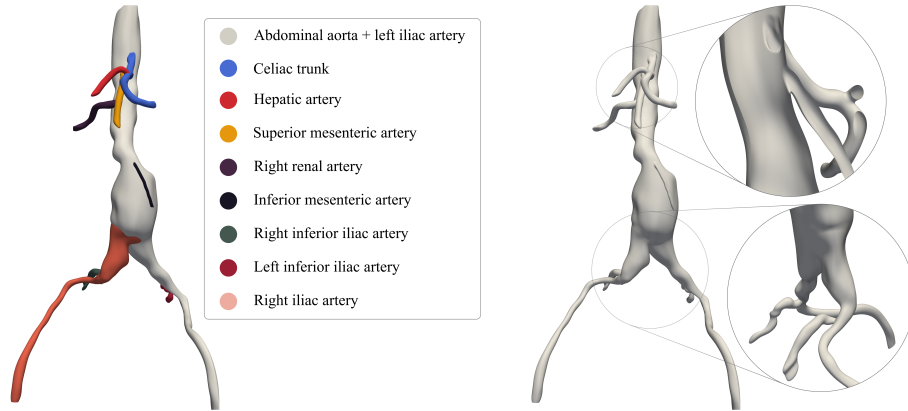


Fig. 5: Subdomains of separate INRs, indicated by different colours (left) and smooth blending of these INRs, with an inside-view at the top (right).

4 Discussion and Conclusion

In this work, we have shown the value of INRs for 3D vascular modeling. We have demonstrated that INRs can be used to fit surfaces in abdominal aortic aneurysms using a small number of annotated points on the surface. Moreover, results show that fitting multiple nested surfaces in one INR is less likely to lead to violation of anatomical priors. Finally, we have used simple arithmetics to blend multiple surfaces represented in INRs into one complex vascular model.

Following the work of [10], we have shown that we can reconstruct continuous surfaces based on (small) point clouds, where their implicit prior leads to surfaces that are smooth and interpolate well in space. This contrasts with, e.g., slice interpolation as is often used to obtain dense voxel masks. INRs are *continuous*, allowing us to represent the vessel surface at any arbitrary resolution. This could facilitate seamless blending of separate arteries for, e.g., CFD analysis [14].

We have demonstrated how a single INR can simultaneously parametrise multiple nested surfaces in an abdominal aortic aneurysm. We showed that using a single INR to represent nested shapes benefits the consistency of the surfaces. The SDF values of nested shapes are similar, as they differ by a local offset. Using a single network to reconstruct them enables the network to learn these offsets by sharing weights and information from the other shapes during training. This nested property is, however, not a topological guarantee, but can be enforced by additional regularisation in the loss function.

Explicit representations such as polygonal meshes [2, 3, 15] and voxel masks are ubiquitous in vascular modeling. INRs could be integrated as an underlying, general, representation of shapes. While they can be easily transformed into meshes or voxel masks at any desirable resolution, the inverse transform is challenging (Fig. 1). For example, while shape arithmetic on mesh representations is cumbersome [13], we have shown that it is straightforward with INRs.

One limitation of INRs is their lack of generalisation; a new INR needs to be optimised for each shape. This may be overcome by enriching the network input with a latent code, in which case INRs could represent a whole distribution of shapes [22]. Alternatively, INRs could be embedded in existing deep learning methods for (cardiovascular) image segmentation, e.g., by including local image features [7] or training hypernetworks [25]. Finally, our work could lead to interactive annotation tools. The combination of recently proposed rapid INR fitting approaches [21] and uncertainty quantification [8] could guide the annotator to areas that need additional annotations.

In conclusion, INRs are a versatile surface representation that are easily acquired and integrated in existing frameworks for vascular modeling.

References

1. Amiranashvili, T., Lüdke, D., Li, H., Menze, B., Zachow, S.: Learning Shape Reconstruction from Sparse Measurements with Neural Implicit Functions. In: MIDL (2022)
2. Antiga, L., Piccinelli, M., Botti, L., Ene-Iordache, B., Remuzzi, A., Steinman, D.A.: An image-based modeling framework for patient-specific computational hemodynamics. *MBEC* **46**(11), 1097–1112 (2008)
3. Arthurs, C.J., Khlebnikov, R., Melville, A., Marčan, M., Gomez, A., Dillon-Murphy, D., Cuomo, F., Silva Vieira, M., Schollenberger, J., Lynch, S.R., et al.: CRIMSON: An open-source software framework for cardiovascular integrated modelling and simulation. *PLoS Comp. Biol.* **17**(5), e1008881 (2021)
4. van Bommel, C.M., Spreeuwiers, L.J., Viergever, M.A., Niessen, W.J.: Level-set based carotid artery segmentation for stenosis grading. In: International Conference on MICCAI. pp. 36–43. Springer (2002)
5. Carr, J.C., Fright, W.R., Beatson, R.K.: Surface interpolation with radial basis functions for medical imaging. *IEEE Trans Med Imaging* **16**(1), 96–107 (1997)
6. Chen, C., Qin, C., Qiu, H., Tarroni, G., Duan, J., Bai, W., Rueckert, D.: Deep learning for cardiac image segmentation: a review. *Front. cardiovasc. med.* **7**, 25 (2020)
7. Chen, Y., Liu, S., Wang, X.: Learning continuous image representation with local implicit image function. In: CVPR. pp. 8628–8638. IEEE/CVF (2021)
8. Gal, Y., Ghahramani, Z.: Dropout as a Bayesian approximation: Representing model uncertainty in deep learning. In: ICML. pp. 1050–1059. PMLR (2016)
9. Gansca, I., Bronsvort, W.F., Coman, G., Tambulea, L.: Self-intersection avoidance and integral properties of generalized cylinders. *Comput. Aided Geom. Des.* **19**(9), 695–707 (2002)
10. Gropp, A., Yariv, L., Haim, N., Atzmon, M., Lipman, Y.: Implicit geometric regularization for learning shapes. In: ICML. pp. 3789–3799 (2020)
11. Hong, Q., Li, Q., Wang, B., Tian, J., Xu, F., Liu, K., Cheng, X.: High-quality vascular modeling and modification with implicit extrusion surfaces for blood flow computations. *Comput Methods Programs in Biomed* **196**, 105598 (2020)
12. Inigo Quilez: Smooth minimum (2013), <https://www.iquilezles.org/www/articles/smin/smin.html>, accessed on 16/02/2022
13. Jiang, X., Peng, Q., Cheng, X., Dai, N., Cheng, C., Li, D.: Efficient booleans algorithms for triangulated meshes of geometric modeling. *Comput. Aided Des. Appl.* **13**(4), 419–430 (2016)

14. Kretschmer, J., Godenschwager, C., Preim, B., Stamminger, M.: Interactive patient-specific vascular modeling with sweep surfaces. *IEEE Trans Vis Comput Graph* **19**(12), 2828–2837 (2013)
15. Lan, H., Updegrove, A., Wilson, N.M., Maher, G.D., Shadden, S.C., Marsden, A.L.: A re-engineered software interface and workflow for the open-source SimVascular cardiovascular modeling package. *J. Biomech. Eng.* **140**(2) (2018)
16. Litjens, G., Ciompi, F., Wolterink, J.M., de Vos, B.D., Leiner, T., Teuwen, J., Išgum, I.: State-of-the-art deep learning in cardiovascular image analysis. *JACC: Cardiovasc. imaging* **12**(8 Part 1), 1549–1565 (2019)
17. Lorigo, L.M., Faugeras, O.D., Grimson, W.E.L., Keriven, R., Kikinis, R., Nabavi, A., Westin, C.F.: Curves: Curve evolution for vessel segmentation. *Med. Image Anal.* **5**(3), 195–206 (2001)
18. Martel, J.N., Lindell, D.B., Lin, C.Z., Chan, E.R., Monteiro, M., Wetzstein, G.: Acorn: adaptive coordinate networks for neural scene representation. *ACM Trans. Graph.* **40**(4), 1–13 (2021)
19. Mildenhall, B., Srinivasan, P.P., Tancik, M., Barron, J.T., Ramamoorthi, R., Ng, R.: Nerf: Representing scenes as neural radiance fields for view synthesis. In: *ECCV*. pp. 405–421. Springer (2020)
20. Mistelbauer, G., Rössl, C., Bäumlner, K., Preim, B., Fleischmann, D.: Implicit modeling of patient-specific aortic dissections with elliptic fourier descriptors. In: *Comput Graph Forum*. vol. 40, pp. 423–434. Wiley Online Library (2021)
21. Müller, T., Evans, A., Schied, C., Keller, A.: Instant Neural Graphics Primitives with a Multiresolution Hash Encoding. *arXiv:2201.05989* (2022)
22. Park, J.J., Florence, P., Straub, J., Newcombe, R., Lovegrove, S.: DeepSDF: Learning Continuous Signed Distance Functions for Shape Representation. In: *CVPR*. pp. 165–174. IEEE/CVF (2019)
23. Schumann, C., Oeltze, S., Bade, R., Preim, B., Peitgen, H.O.: Model-free surface visualization of vascular trees. In: *EuroVis*. pp. 283–290 (2007)
24. Shani, U., Ballard, D.H.: Splines as embeddings for generalized cylinders. *Comput. Vis., Graph, and Image Process.* **27**(2), 129–156 (1984)
25. Sitzmann, V., Chan, E.R., Tucker, R., Snavely, N., Wetzstein, G.: MetaSDF: Meta-Learning Signed Distance Functions. In: *NeurIPS* (2020)
26. Sitzmann, V., Martel, J.N., Bergman, A.W., Lindell, D.B., Wetzstein, G.: Implicit Neural Representations with Periodic Activation Functions. In: *NeurIPS* (2020)
27. Sobocinski, J., Chenorhokian, H., Maurel, B., Midulla, M., Hertault, A., Le Roux, M., Azzaoui, R., Haulon, S.: The benefits of EVAR planning using a 3D workstation. *Eur J Vasc Endovasc Surg* **46**(4), 418–423 (2013)
28. Sun, Y., Liu, J., Xie, M., Wohlberg, B., Kamilov, U.S.: Coil: Coordinate-based internal learning for tomographic imaging. *IEEE Trans Comput Imaging* **7**, 1400–1412 (2021)
29. Tran, K., Yang, W., Marsden, A., Lee, J.T.: Patient-specific computational flow modelling for assessing hemodynamic changes following fenestrated endovascular aneurysm repair. *JVS: Vascular Science* **2**, 53–69 (2021)
30. Wilson, N.M., Ortiz, A.K., Johnson, A.B.: The vascular model repository: a public resource of medical imaging data and blood flow simulation results. *J. Med. Devices* **7**(4) (2013)
31. Wittek, A., Mufty, H., Catlin, A., Rogers, C., Saunders, B., Sciarrone, R., Fourneau, L., Meuris, B., Tavner, A., Joldes, G.R., et al.: Image, geometry and finite element mesh datasets for analysis of relationship between abdominal aortic aneurysm symptoms and stress in walls of abdominal aortic aneurysm. *Data Br.* **30**, 105451 (2020)

32. Wolterink, J.M., Zwienerberg, J.C., Brune, C.: Implicit Neural Representations for Deformable Image Registration. In: MIDL. PMLR (2022)
33. Wu, J., Ma, R., Ma, X., Jia, F., Hu, Q.: Curvature-dependent surface visualization of vascular structures. *Computerized Medical Imaging and Graphics* **34**(8), 651–658 (2010)
34. Zhu, C., Leach, J.R., Wang, Y., Gasper, W., Saloner, D., Hope, M.D.: Intraluminal thrombus predicts rapid growth of abdominal aortic aneurysms. *Radiology* **294**(3), 707–713 (2020)